PCCP

ROYAL SOCIETY OF CHEMISTRY

PERSPECTIVE

View Article Online
View Journal

Cite this: DOI: 10.1039/d6cp00961a

Probing hydration-driven ion recognition using cryogenic ion trap infrared spectroscopy

Keisuke Hirata, *[a] James M. Lisy, [bc] Masaaki Fujii [bd] and Shun-ichi Ishiuchi*[a]

Ion recognition, in which a molecule (ionophore) binds to a selected ion, is one of the fundamental chemical and biological phenomena controlled by an intricate balance among ions, ionophores, and solvents. To date, however, the molecular-level understanding of ion recognition remains elusive due to the difficulty in directly probing solvation structures. Recent advances in gas-phase cryogenic ion trap spectroscopy have enabled us to probe the structural evolution of the micro-solvated ion-ionophore complexes, providing a benchmark for solvation effects on ion recognition. In this perspective, we review recent progress in elucidating the hydration-driven ion recognition phenomena using cryogenic double ion trap infrared spectroscopy, primarily focusing on prototypical ionophores, valinomycin, 18-crown-6, and beauvericin. Our findings reveal the critical roles of water in the ion selectivity of structurally flexible ionophores, for which molecular mechanisms cannot be rationalized by conventional understanding based on the size-matching model. We also focus on the future of cryogenic ion spectroscopy to study the chemistry of functional molecules.

Received 16th March 2026,
Accepted 11th May 2026

DOI: 10.1039/d6cp00961a

rsc.li/pccp

[a] Department of Chemistry, School of Science, Institute of Science Tokyo, 2-12-1 4259 Ookayama, Meguro-ku, Tokyo 152-8550, Japan. E-mail: hirata.k.c502@m.isct.ac.jp, ishiuchi.s.94d6@m.isct.ac.jp
[b] International Research Frontiers Initiative (IRFI), Institute of Integrated Research, Institute of Science Tokyo, 4259 Nagatsuta-cho, Midori-ku, Yokohama 226-8503, Japan
[c] Department of Chemistry, University of Illinois at Urbana-Champaign, Urbana, Illinois 61801, USA
[d] Research and Development Initiative, Chuo University, 1-13-27 Kasuga, Bunkyo-ku, Tokyo 112-8551, Japan

1. Introduction

Ion recognition, in which a molecule binds to a selected ion, is one of the most fundamental processes in a wide field of chemistry and biology, including catalysis (enzymes),[1] analytical sensing, ion transport through channels and transporters, and signal transduction in biological systems. Understanding the underlying principles of ion selectivity is therefore essential

Keisuke Hirata

Keisuke Hirata is an Assistant Professor of the Department of Chemistry at the Institute of Science Tokyo. He received his PhD degree from the University of Tokyo in 2019 under the supervision of Professor Tatsuya Tsukuda and has been an Assistant Professor at the Institute of Science Tokyo. His research interests include gas-phase experimental techniques in infrared and ultraviolet spectroscopy, with particular focus on hydration effects on molecular functions such as ion recognition.

James M. Lisy

Professor James M. Lisy is currently a Specially Appointed Professor in the Laboratory for Future Interdisciplinary Research of Science and Technology (FIRST) and the Institute of Integrated Research (IIR) at the Institute of Science Tokyo. He received his PhD from Harvard University in 1979, under the direction of Prof. William Klemperer, and was a post-doctoral associate of Prof. Y.T. Lee from 1979 to 1981. He was a Professor of Chemistry at the University of Illinois Urbana-Champaign from 1981 to 2011. He has been a program officer at the US National Science Foundation and a visiting or guest professor in France, Japan, and Denmark.

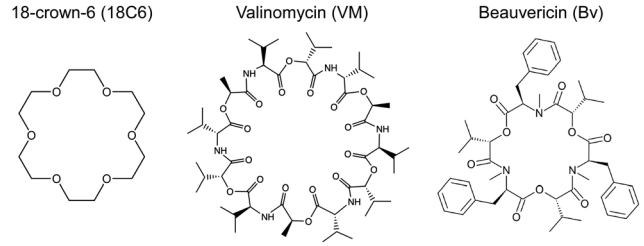

Fig. 1 Molecular structures of ionophores studied in our group.

for elucidating (bio-)molecular functions, also paving the way for the rational design of ion-selective molecules (ionophores). Traditionally, ion recognition has been interpreted within the framework of the "size-matching" model, in which ion selectivity arises from the structural complementarity between an ion and the cavity of a host molecule. Although this simple and intuitive model accounted for many experimental observations, it is increasingly evident that the size-matching concept alone is insufficient to describe the complexity of ion selectivity.

A representative example is provided by one of the most prototypical ionophores, 18-crown-6 ether (18C6, Fig. 1).[2] 18C6 shows the highest affinity to K^+ among alkali metal ions in aqueous solution (Fig. 2, red),[3,4] which was ascribed to the optimal size matching of K^+ and 18C6. In contrast, gas-phase binding energies monotonically increase with the contraction in ionic size (Fig. 2, blue), indicating a preference for smaller ions.[5] This apparent contradiction between aqueous and gas phases clearly demonstrates the critical effects of hydration on ion selectivity. Because alkali ions are strongly hydrated in aqueous solution with 200–500 kJ mol^{-1} of predicted energetic gain,[6] the energetic cost of dehydration when encapsulated by ionophores must play a crucial role in ion recognition. It remains unclear, however, as to how water microscopically

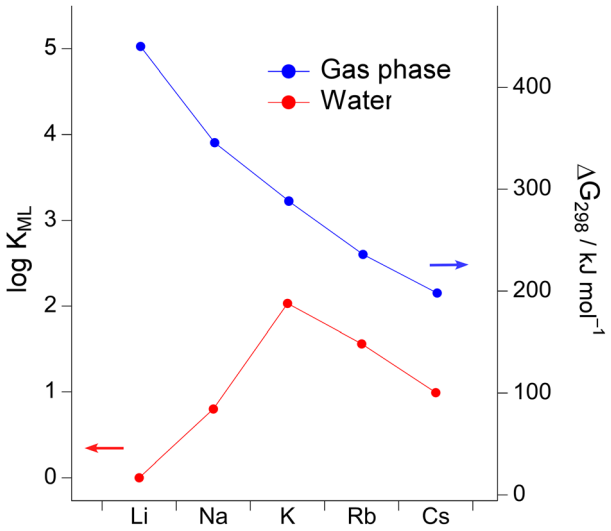

Fig. 2 Binding constants (red) of 18-crown-6 (18C6) with alkali metal ions in aqueous solution and calculated gas-phase binding (Gibbs free) energies (blue) with alkali metal ions at the M06-2X/6-311++G(d,p) level. Adapted with permission from ref. 49. Copyright 2025 American Chemical Society.

affects the ion-ionophore binding motifs and thereby gives rise to ion selectivity. This is largely due to the lack of direct experimental information on molecular-level hydration structures.

Hydration not only affects the thermodynamic selectivity but also the kinetics of ion transport. Ionophores capture ions at the water–membrane interface, translocate them through the hydrophobic cell membrane, and release them on the opposite side (Fig. 3). These catch and release processes are likely affected by hydration as they involve dehydration (or re-hydration) of ions. Molecular dynamics (MD) simulations of

Masaaki Fujii

Masaaki Fujii is appointed as a Professor of Chuo U in 2024 via the Professor of Tokyo Institute of Technology in 2003, Professor of Institute for Molecular Science, Associate Professor of Waseda U, Assistant Professor of Tohoku U and Visiting Scientist of Cornell U. He received Dr Sci. from Tohoku U in 1987. He has been studying spectroscopy and dynamics of isolated molecules and clusters by developing novel multicolor laser spectroscopy including picosecond time-resolved UV-UV-IR spectroscopy. He was awarded by the Chemical Society of Japan (2014), The Spectroscopical Society of Japan (2015), Japan Society for Molecular Science (2018) and Humboldt Foundation (2019).

Shun-ichi Ishiuchi

Shun-ichi Ishiuchi is a Professor in the Department of Chemistry at the Institute of Science Tokyo, Japan. He received his PhD from the Graduate University for Advanced Studies (SOKENDAI) at Institute for Molecular Science in 2001. His research focuses on molecular spectroscopy and gas-phase cluster science, combining cryogenic ion spectroscopy with quantum chemistry calculations to elucidate solvation effects and molecular recognition. He has developed advanced laser spectroscopic methods to probe microsolvation, ion selectivity, and excited-state dynamics of biomolecular ions. He has authored numerous influential publications and received several awards, including the Molecular Science Society International Award (2019).

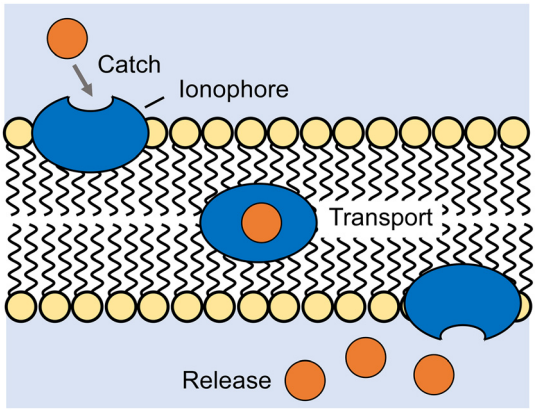

Fig. 3 Schematic of ion transport by carrier-type ionophores.

ion transport at the water–oil interfaces suggest that the free-energy barrier for the translocation between water and oil phases is lowered by transient hydration called "water fingers" at the interface.[7] In a similar context, MD simulations of ionophores suggest that ion release can be triggered by the attachment of only a few water molecules, implying that the transient fluctuating hydration events at the water–membrane interface facilitate the catch and release processes. These computational findings necessitate experimental approaches capable of resolving kinetic hydration effects on ion transport. However, at this moment, interface spectroscopy is not sensitive enough to probe these interesting but rare encounters of ions and ionophores.

A powerful methodology to investigate these hydration effects is the study of hydrated clusters, which consist of ion–ionophore complexes hydrated by a well-defined number of water molecules. Gas-phase infrared (IR)/ultraviolet (UV) spectroscopy coupled with the supersonic jet technique[8,9] has revealed numerous molecular structures and H-bond networks of hydrated clusters by measuring high-resolution IR/UV spectra at low temperatures, which cannot be obtained by conventional solution-phase spectroscopy. However, the supersonic jet technique is difficult to be applied to larger biomolecules because they decompose due to the heat required to evaporate them. Although alternative cluster-generation techniques,[10] such as laser ablation,[11–15] were explored, their applicability to functional biomolecules remained limited.

A breakthrough was achieved by Rizzo and co-workers in 2006 by combining electrospray ionization (ESI) with the cryogenic ion trapping technique.[16] ESI,[17] known as a soft ionization method, enables biomolecules to be transferred to from the solution to gas-phase without degradation, while cryogenic ion trapping allows for efficient cooling and high-resolution IR/UV spectroscopy. Thus, ESI cryogenic ion trap spectroscopy[16,18–28] has drastically expanded the scope of gas-phase spectroscopy to large biologically relevant molecules inaccessible by conventional techniques. Further advances in ESI ion trap spectroscopy have been made after this work. One is the employment of a second ion trap,[29,30] in which solvated clusters are efficiently produced under controlled thermal conditions prior to the first spectroscopic cryotrap. This technique called "dual" ion trap spectroscopy enables the spectroscopic studies of well-defined solvated clusters,[29,30] suitable for investigating the hydration effects on ion recognition.

In this perspective, we summarize our recent advances in microscopic hydration effects in ion recognition, with a particular focus on insights gained from double ion trap spectroscopy. We also highlight the complementary role of computational approaches and discuss prospects, including the implications for molecular design of functional materials and for elucidating biologically relevant ion selectivity.

2. ESI cryogenic ion trap spectroscopy

The concept of combining ESI with a cryotrap dates back to the pioneering work by the Weinkauf group.[31] In 2004, they reported the UV photodissociation (UVPD) spectrum of protonated tryptophan trapped in an ion trap cooled at the liquid-nitrogen temperature. Unfortunately, the UV spectrum was broad, which was initially attributed to insufficient cooling, but was later ascribed to lifetime broadening due to the ultrafast relaxation of the photo-excited state.[32] Two years later, Rizzo and co-workers reported the sharp UVPD spectra of protonated tyrosine using a linear 22-pole ion trap,[16] demonstrating the potential of ESI cryogenic ion trap spectroscopy. At that time, higher order multi-pole ion traps were employed instead of a 3D quadrupole ion trap (QIT) for cryogenic spectroscopy because ions confined in QITs were believed to undergo thermal excitations by radio frequency (RF) potential, which is called RF heating.[33] In fact, Choi *et al.* reported an effective vibrational temperature of $\sim$50 K for protonated tyrosine in the 3D QIT even though the electrodes of the QIT are cooled down to $\sim$4 K.[33] However, our group revealed that the RF heating in QITs is not the primary cause of ion cooling and that the high thermal conductivity of the trap electrodes is more crucial for effective cooling.[34] In particular, the vibrational temperature of trapped ions is drastically decreased from $\sim$50 K to $\sim$10 K by replacing the stainless-steel QIT electrodes with the one fabricated from copper as the buffer gas is more efficiently cooled by the He refrigerator due to the high thermal conductivity of the copper electrodes prior to exiting the QIT. We now employ the copper-made QIT as a spectroscopic cryotrap as its steep potentials enable narrow ion confinement and excellent compatibility with laser spectroscopy. Gas-phase spectroscopy often suffers from low ion densities, hampering conventional transmission measurements. Instead, we employ the tagging technique, in which IR absorption is measured by the dissociation of a weakly bound inert atom/molecule ("tag").[19] We use molecular hydrogen (H_2) as a tag due to its minimal perturbation of the vibrational frequencies of the hydrated ion-ionophore complexes.

The use of the second ion trap for the production of hydrated clusters was first reported by Garand's group.[29] Although hydrated clusters can also be generated directly in the ESI source,[35] this methodology has difficulty in efficient and stable production of hydrated clusters due to susceptibility

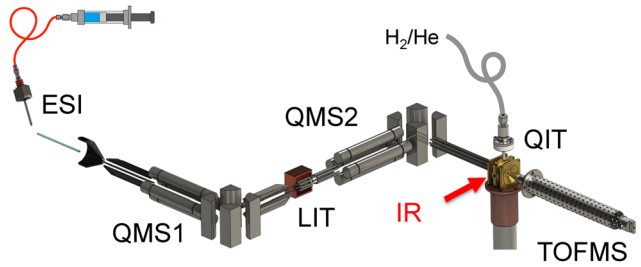

Fig. 4 Experimental setup of the ESI double ion trap spectroscopy and the schematic of the H_2-tagging technique. ESI: electrospray ionization, QMS: quadrupole mass spectrometer, LIT: linear ion trap, QIT: quadrupole ion trap, TOFMS: time-of-flight mass spectrometer. Adapted with permission from ref. 30. Copyright 2021 American Chemical Society.

to ESI conditions such as humidity and temperature.[29,36] The use of the second ion trap solves the issue and is a versatile method for cluster generation.

Our experimental setup has an ESI source, a spectroscopic ion trap (QIT), and a second ion trap (LIT) for cluster production (Fig. 4).[30,34] Methanol solutions containing an ionophore and alkali metal/alkaline earth chloride are electrosprayed through a heated capillary (60–70 °C) to facilitate desolvation. Ions thus produced are collected by an ion funnel and mass-selected by a quadrupole mass spectrometer (QMS1) before entering the LIT. Water vapor is introduced into the LIT (70–120 K) to produce hydrated clusters. The hydrated clusters are mass-selected by a second quadrupole mass spectrometer (QMS2) and guided to the cryogenic QIT maintained at 4 K. A mixture of H_2/He buffer gas is introduced into the QIT and the trapped ions are cooled down at ~10 K (vibrational temperature) by collisions with the buffer gas. H_2 is condensed onto the cold ions, forming van der Waals complexes. The H_2-tagged ions are then irradiated with a tunable IR laser, which dissociates the weakly bound H_2 from the parent ions. The IR photodissociation (IRPD) spectrum is measured by monitoring the photofragment signals with a time-of-flight mass spectrometer (TOFMS) as a function of the IR photon energy.

3. Ion recognition of ionophores

3.1. Thermodynamic effects

3.1.1. Valinomycin. Valinomycin (VM, Fig. 1) is one of the most representative naturally occurring ionophores and was first isolated in 1955[37] before the synthesis of the famous crown ethers. VM consists of alternating ester and amide bonds (Fig. 1) and selectively transports K^+ ions across the cell membrane, exhibiting antitumor, antiviral, antibacterial, and antifungal activities,[38] as well as being used in ion-selective electrodes.[39] In polar solvents such as methanol, VM displays high affinity for K^+, Rb^+, and Cs^+ with comparable binding constants, whereas its binding constants for Na^+ and Li^+ are ~10^{-4} times smaller: Rb^+ (5.26 for log$K$), K^+ (4.90), Cs^+ (4.41) ≫ Na^+ (0.67), Li^+ (<0.7).[4] X-ray crystallographic studies revealed that in the VM-K^+ complex (hereafter denoted K^+VM), VM adopts a symmetric (C_3) "bracelet" structure, where K^+ is coordinated by ester carbonyl oxygens in a nearly octahedral geometry (Fig. 5).[40] The backbone of VM is folded in a β-turn-like manner, forming six intramolecular H-bonds between an amide NH and an amide CO.

The ion selectivity of VM has been conventionally described by the size-matching model using MD simulations and density functional theory (DFT) calculations.[41] Varma and co-workers calculated the binding energies of metal ions with VM and found that the binding energy of Na^+VM is 12 kcal mol^{-1} larger than that of K^+VM, despite the larger binding constant of K^+VM in polar solvents.[41] This apparent contradiction is partly resolved by considering hydration: the dehydration energy required for Na^+ is 21 kcal mol^{-1} larger than that for K^+, suggesting an energetic favor to K^+ over Na^+ by 9 kcal mol^{-1}. This energetic relationship is ascribed to the size match between K^+ and the cavity of VM.

However, the calculated conformation of Na^+VM (bracelet structure) seems contradictory to that reported[42,43] in a polar solvent in which Na^+ is coordinated by <6 ester COs. This inconsistency would be ascribed to the drawbacks of the theoretical and/or experimental methods. The theoretical calculations assume a continuous medium with a certain permittivity, neglecting the molecular nature of solvent molecules.[41,44,45] On the other hand, experimental results could be severely contaminated by bare VM uncomplexed to low-affinity Na^+. In any case, clearer structural information is needed to describe the role of hydration in the thermodynamic K^+ selectivity of VM.

Fig. 6 shows the IRPD spectra of the bare VM-alkali metal complexes.[46] The spectral features of Li^+VM substantially differ from those of the other complexes. On the other hand, the spectral features of M^+VM (M^+ = Na^+–Cs^+) are markedly similar, indicating that these complexes adopt closely related molecular structures. For the four complexes, both the NH stretches (colored in orange in Fig. 6) and ester CO stretches (blue) appear as single bands, while the amide CO stretches (light green) have a major band accompanied by a shoulder. Given that VM contains six amide and ester C═Os, these spectral features indicate a highly symmetric structure. The NH stretch bands are systematically blue-shifted with increasing ionic radius. Indeed, these features are well reproduced by the calculated IR spectrum of the lowest-energy C_3-symmetric bracelet conformers (Fig. 6). The blue-shift of the NH stretches

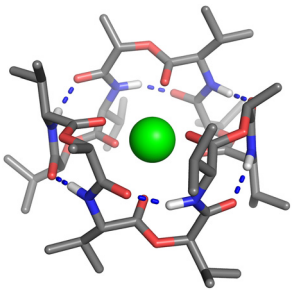

Fig. 5 Crystal structure of K^+VM (gray = C, blue = N, red = O, white = H, purple = K). Blue dotted lines show intramolecular H-bonds. Hydrogen atoms other than the NH bonds were omitted for clarity. Adapted with permission from ref. 47. Copyright 2023 American Chemical Society.

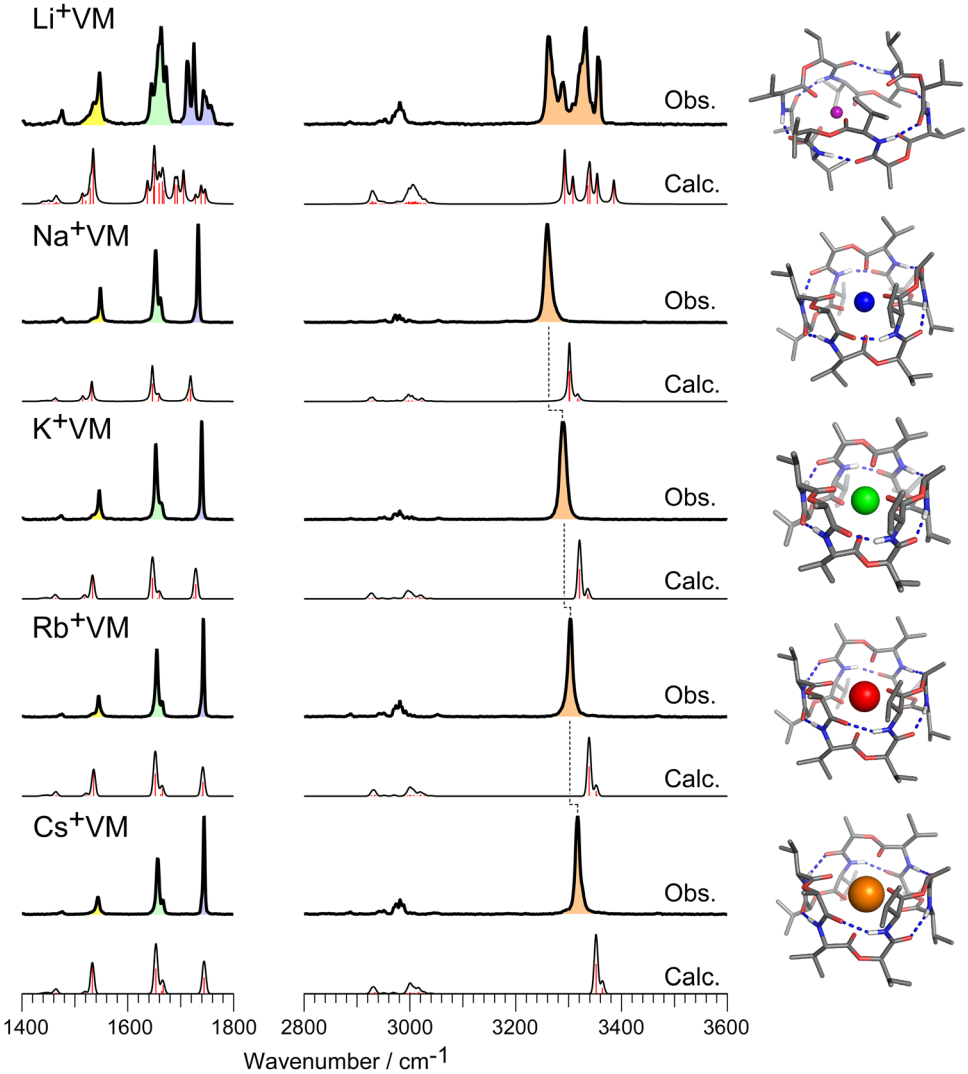

Fig. 6 IRPD spectra of M^+VM (M^+ = Li^+, Na^+, K^+, Rb^+, Cs^+). The calculated IR spectra of the lowest-energy conformers are also shown with the molecular geometries. The black solid curves in the calculated spectra are made by convolution of stick red lines. Color-coded bands correspond to certain vibrational signatures (orange = NH stretch, blue = OH stretch, blue = ester CO stretch, light green = amide CO stretch, yellow = NH bend). Adapted with permission from ref. 46. Copyright 2023 Royal Society of Chemistry.

reflects an elongation of the intramolecular H-bonds within the bracelet structure. These observations demonstrate that VM can accommodate ions with a wide range of ionic radii from Na^+ (0.95 Å) to Cs^+ (1.69 Å), retaining its bracelet conformation. In other words, the bracelet conformation of VM intrinsically has the flexibility to bind ions with a wide range of sizes, probably due to the elongation/contraction of intramolecular H-bonds in the β-turn-like folded structure. For the Li^+VM complex, the spectral features of the split band of the amide NH and ester/amide C═O bands indicate the breakdown of C_3 symmetry. The structure is assigned to a non-symmetric lowest-energy conformation (Fig. 6), in which Li^+ is displaced from the cavity center, due to the size mismatch with VM. The low affinity of VM to Li^+ in solution is ascribed to this distorted conformation.

While these experimental results in the absence of solvent well rationalize the low affinity of VM to Li^+, they raise a fundamental question as to why Na^+ has much less affinity to VM. To address the role of hydration, the IRPD spectra of $M^+VM(H_2O)_1$ (M^+ = Na^+, K^+) were measured using the H_2-tagging method (Fig. 7a).[30,47] The vibrational bands in the 3200–3400 cm^{-1} and 3400–3700 cm^{-1} ranges were assigned to the amide NH (orange) and water OH (blue) stretches, respectively. For $K^+VM(H_2O)_1$, the NH stretches remain essentially unchanged upon hydration, indicating the preservation of the symmetric bracelet structure. In contrast, $Na^+VM(H_2O)_1$ exhibits a prominent splitting of the NH stretches, demonstrating the breakdown of the symmetric bracelet structure even by single water hydration. Another distinct difference is in the OH stretch range: $Na^+VM(H_2O)_1$ shows intense bands at 3497 cm^{-1} (symmetric) and 3598 (antisymmetric) cm^{-1}, though the corresponding OH stretches are relatively weak for $K^+VM(H_2O)_1$. The symmetric OH stretch of water is found to be enhanced when water is directly bonded to a cation.[48] These spectral observations strongly suggest that water is inserted into the cavity and is

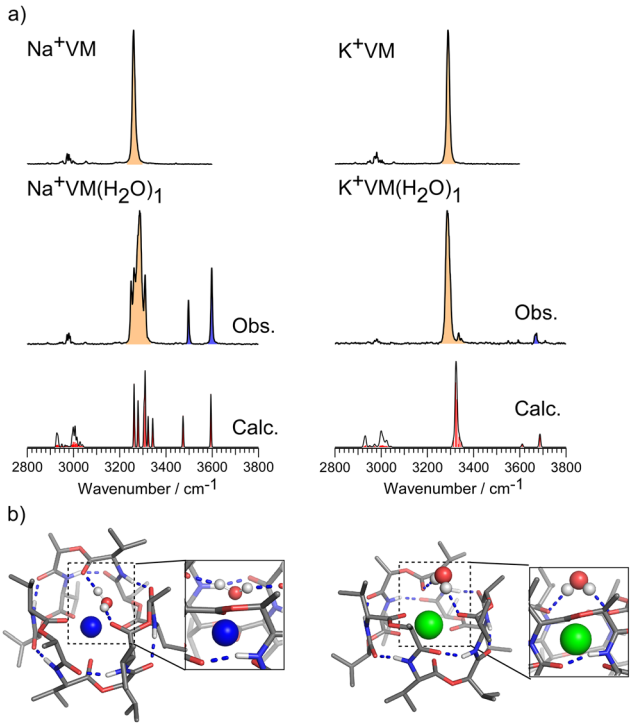

Fig. 7 (a) IRPD spectra of $M^+VM(H_2O)_n$ (M^+ = Na^+, K^+; n = 0, 1). Color codes show the region of the vibrational signatures (orange = NH stretch, blue = OH stretch). The calculated IR spectra of the lowest-energy conformers are also shown with (b) molecular geometries. Adapted with permission from ref. 47. Copyright 2023 American Chemical Society.

directly bonded to Na^+, thereby distorting the backbone of VM. The calculated spectrum of the lowest-energy conformer well reproduces the experimental IRPD spectra (Fig. 7a), supporting this hypothesis. In the assigned structure, water is directly coordinated to Na^+, reducing the coordination number of Na^+ to VM. Interestingly, the positions of the water molecule differ between the two complexes: water resides outside the cavity in $K^+VM(H_2O)_1$, whereas water penetrates into the cavity and directly binds to Na^+ (Fig. 7b).

This led us to check whether these differences were retained upon further hydration, $M^+VM(H_2O)_n$ (M^+ = Na^+, K^+; n = 2–10) (Fig. 8).[47] For $Na^+VM(H_2O)_n$, all spectra display split and broadened NH stretches (3240–3360 cm^{-1}) and amide/ester CO stretches (1640–1680 cm^{-1}, 1720–1770 cm^{-1}) as observed in the monohydrate. In contrast, the IRPD spectra of $K^+VM(H_2O)_n$ show relatively sharp NH and amide/ester CO bands over the same hydration range. These observations show that the hydration-induced distorted conformation is retained with Na^+VM, while K^+VM undergoes a minimal conformational change upon further hydration.

In summary, the low affinity of Na^+ to VM can be ascribed to the strong conformational distortion of the Na^+VM induced by water penetration. This effect is driven by the higher charge density of Na^+, which favors direct coordination by water due to a stronger electrostatic interaction. The conformations of hydrated Na^+VM revealed here significantly differ from those calculated using a continuum dielectric model,[41] underscoring the importance of the intrinsic molecular nature of solvent, such as the capability of H-bonding. These findings challenge the traditional size-matching model, which treats ion recognition as a simple two-body interaction between a host and a guest. Instead, ion recognition in flexible molecular systems such as VM can be governed by the interplay among the host, the guest, and water.

3.1.2. 18-Crown-6 ether. Hydration effects, as observed in VM, may play a significant role in other ionophores as well. To explore this possibility, we investigated the micro-hydration effects on ion recognition by crown ethers, a major class of synthetic ionophores.[49] As described in the Introduction, 18-crown-6 ether

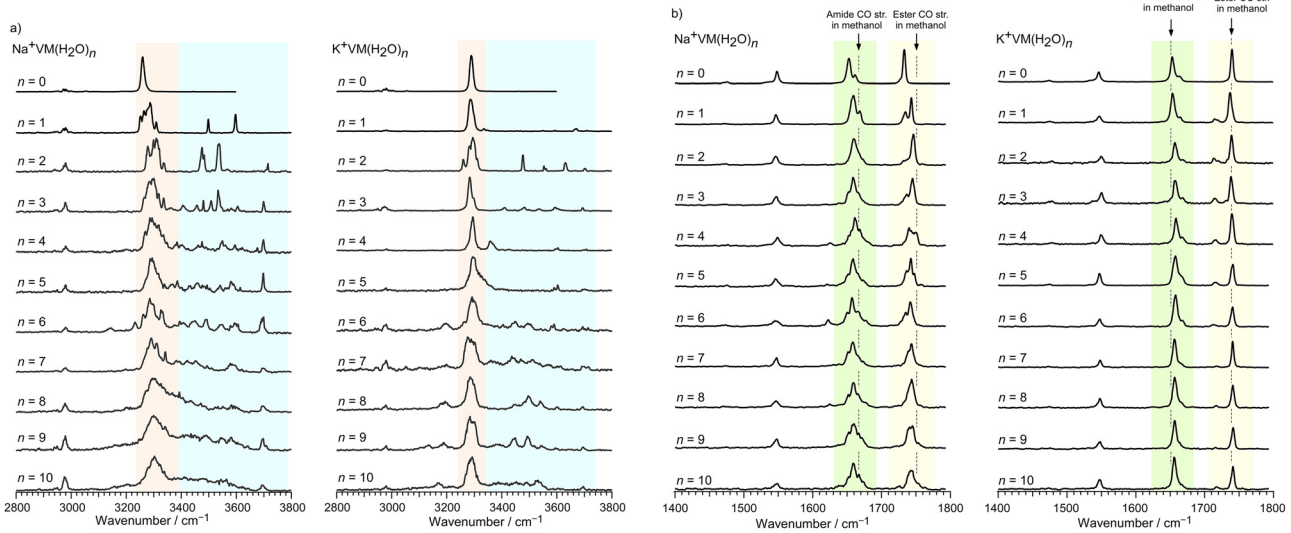

Fig. 8 IRPD spectra of $M^+VM(H_2O)_n$ (M^+ = Na^+, K^+; n = 0–10) in the (a) 3 μm and (b) 6 μm ranges. Color codes show the region of the vibrational signatures (orange = NH stretch, cyan = OH stretch, yellow = ester CO stretch, light green = amide CO stretch). The dotted lines show corresponding amide/ester CO stretches in methanol solution. Reprinted with permission from ref. 47. Copyright 2023 American Chemical Society.

(18C6) selectively encapsulates K^+ in aqueous solution over the other four alkali metal ions.[3,4] However, the monotonic increase for gas-phase binding energies with increasing ionic sizes (Fig. 2) contradicts the trend for the aqueous-phase binding constants,[4,5] indicating the critical role of hydration in ion selectivity. Pioneering works[50,51] by Lisy and co-workers revealed hydration structures of $M^+18C6(H_2O)_n$ by probing OH stretches; however, they were unable to elucidate the key conformational changes of 18C6 responsible for K^+ selectivity, which necessitates probing characteristic vibrational modes of 18C6 itself. The CH stretches of 18C6 are conformation-sensitive, though their assignments are challenging due to complicated band splitting by anharmonic Fermi resonance with CH_2 bend overtones.[52] In principle, such anharmonic calculations are computationally demanding and thus difficult to apply to large molecules such as 18C6. Sibert and co-workers have developed a practical and reliable theoretical framework for the CH stretch range that accounts for Fermi couplings between local-mode CH stretches and CH_2 bend overtones.[53,54] In our work, we have combined ESI cold ion trap spectroscopy with this anharmonic methodology to probe the hydration-induced structural changes of the M^+18C6 complexes.

Fig. 9 shows the IRPD spectra of M^+18C6 complexes in the CH stretch range.[49] The IRPD spectra of Li^+18C6 and Na^+18C6 show multiple CH bands over 2860–3000 cm^{-1}, indicating a similar conformation of 18C6. In contrast, K^+18C6 exhibits a different spectral pattern featured by concentrated bands at $\sim$2900 cm^{-1}, suggesting a different conformation of 18C6 from Li^+18C6 and Na^+18C6. The anharmonic spectra calculated for the lowest-energy conformers remarkably well reproduce the spectral features of the experimental IRPD spectra mentioned above (Fig. 9). Li^+18C6 and Na^+18C6 have been assigned to "buckled" conformations, in which 18C6 bends to wrap around the smaller cations, whereas K^+18C6 adopts a flat and highly symmetric (D_{3d}) "unbuckled" conformation with an open ring. These differences can be rationalized by the need for the smaller cation to maximize electrostatic interactions with ether oxygen atoms, whereas K^+ can form strong coordination without requiring the crown ether to buckle. These structural assignments are consistent with ion mobility measurements,[55] the IR multiphoton dissociation spectra[56] and previous theoretical calculations[57–59] of bare M^+18C6, but our results provide clearer vibrational signatures for specific conformations of 18C6.

Fig. 10a shows the IRPD spectra of hydrated $M^+18C6(H_2O)_n$ clusters (n = 1–3) in the CH stretch range.[49] For the K^+18C6 complex, the spectral pattern remains substantially unchanged upon hydration, suggesting that the unbuckled structure is preserved up to n = 3. By contrast, Li^+18C6 and Na^+18C6 undergo pronounced spectral changes by hydration. The spectra begin to change by single water addition, and the second water molecule induces a significant change in the IRPD spectra. The CH bands above 2970 cm^{-1} have diminished and the spectra are similar to that of K^+18C6, suggesting a structural transition to the unbuckled structure at n = 2. The transition is complete at n = 3 as the spectra of $M^+18C6(H_2O)_3$ for all three ions are essentially identical, featuring intense bands centered at $\sim$2920 cm^{-1} accompanied by weak bands at $\sim$2840 cm^{-1}, $\sim$2880 cm^{-1}, and $\sim$2950 cm^{-1}. Fig. 10b shows the assigned structures of $M^+18C6(H_2O)_2$. It should be mentioned that these conformations reproduce the experimental spectra of the OH stretch bands as well. The Li^+18C6 and Na^+18C6 undergo unbuckling of the ether ring, in which the ion is located off-center with a reduced coordination number to 18C6, while K^+ remains centered. The

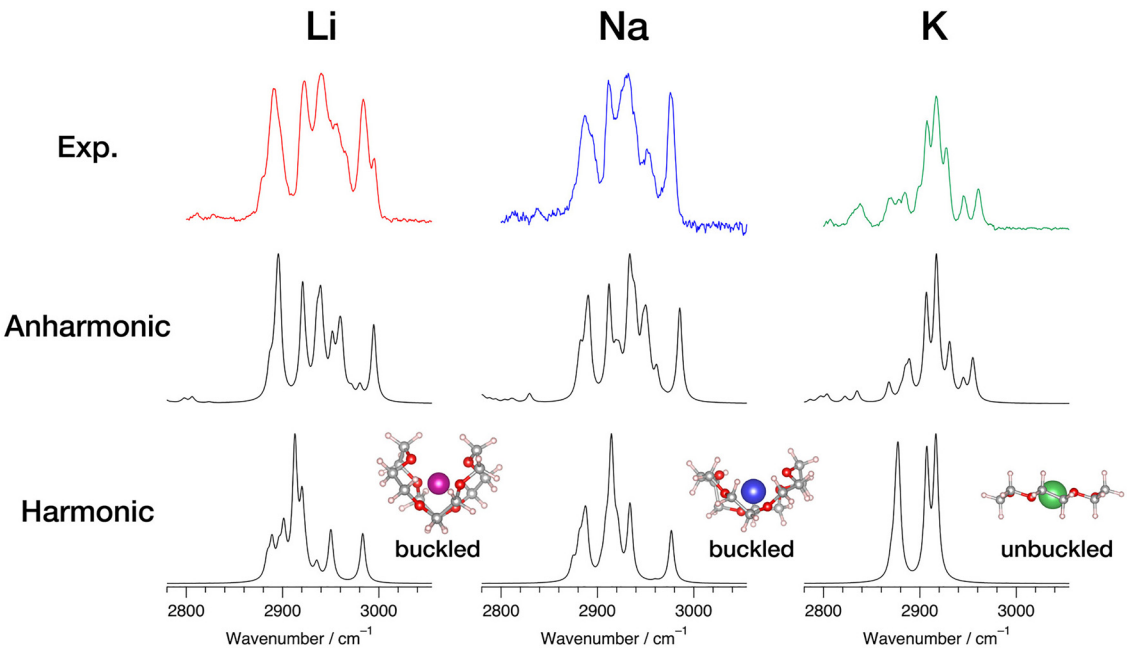

Fig. 9 IRPD spectra of M^+18C6 (M^+ = Li^+, Na^+, K^+) with calculated IR spectra in the CH stretch range. Harmonic spectra were calculated at the B3LYP/6-311++G(d,p) level, scaled by a factor of 0.96. Anharmonic spectra were calculated using the local-mode model Hamiltonian. Reprinted with permission from ref. 49. Copyright 2025 American Chemical Society.

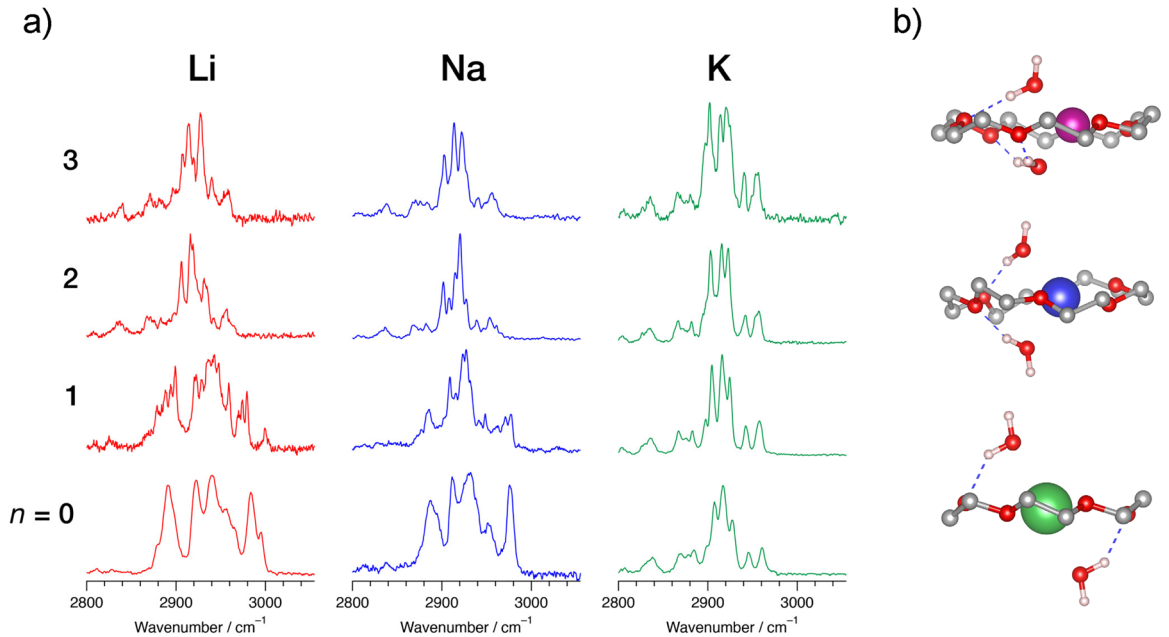

Fig. 10 (a) IRPD spectra of $M^+18C6(H_2O)_n$ ($M^+ = Li^+$, Na^+, K^+; $n = 0–3$) in the CH stretch range. (b) Conformations of $M^+18C6(H_2O)_2$ ($M^+ = Li^+$, Na^+, K^+). Reprinted with permission from ref. 49. Copyright 2025 American Chemical Society.

water molecules are directly bonded to the alkali metal cations and H-bonded to the etheric oxygens. The hydration-induced unbuckling occurs to maximize the interactions between water and 18C6/alkali metal ions. Notably, a wide-angle X-ray scattering study also proposed the off-centered positions of Li^+ and Na^+ and the central position of K^+ of M^+18C6 in aqueous solution,[60] in excellent accordance with our gas-phase experimental observations. These findings indicate that hydration-induced unbuckling reduces the ion binding affinities of Li^+ and Na^+, as K^+ shows an optimal size match with the unbuckled conformation. In this sense, the K^+ selectivity of 18C6 is not dictated by a simple size-matching concept for a rigid ionophore, but is governed by the hydration-induced conformational locking that leads to effective size-matching for a flexible ionophore.

3.1.3. Beauvericin. Beauvericin (Bv) is a naturally occurring ionophore composed of alternating three peptide bonds and ester bonds (Fig. 1).[61] Bv exhibits various biological activities, such as anticancer, anti-inflammatory, and antifungal, and insecticidal effects due to its ionophoric ability to transport metal ions across the cell membrane.[62–65] The nature and mechanism of this ionophoric behavior, however, remained elusive because of ill-defined ion selectivity. To the best of our knowledge, there was no direct experimental determination of binding constants between Bv and alkali or alkaline earth metal ions. Instead, the binding constants were inferred from extraction measurements of ions from an aqueous phase to an organic phase in the following sequence: $K^+ \approx Rb^+ > Na^+ > Li^+$.[66] In contrast, the binding constants determined by a different extraction scheme provide a totally different sequence: $Li^+ > K^+ > Na^+ \approx Rb^+$.[67] In the latter method, the organic phase is saturated with water. Thus, extraction measurements could be highly sensitive to residual water in the organic phase, which alters the thermodynamic stabilities of ions in the organic layer. Furthermore, the binding constants are inferred assuming the formation of a 1 : 1 Bv-metal complex, whereas NMR studies suggested the presence of 2 : 1 (M^+Bv_2) and higher complexes.[68] Therefore, the direct thermodynamic information on the ion selectivity of Bv is needed.

Fig. 11a shows the ESI mass spectrum of 1 : 1 Bv–alkali metal complexes.[69] The mass spectrum was measured for the methanol solution containing the equivalent amounts of Bv and the five alkali metal ions. The five peaks correspond to the five M^+Bv complexes, in which the isotope patterns are qualitatively reproduced by natural isotope abundance. The strongest peak of Na^+Bv indicates an intrinsic preference for Na^+ for the 1 : 1 complex among the five alkali metals in methanol solution, providing the first direct thermodynamic evaluation of the ion selectivity of Bv.

To reveal the mechanism of Na^+ selectivity, we applied the cryogenic IR spectroscopy to each M^+Bv complex (Fig. 12a).[69] The split bands in 1620–1680 cm^{-1} and 1720–1790 cm^{-1} are assigned to amide C=O and ester C=O stretches, respectively, from the analogy to the condensed-phase IR spectra.[68] Provided only two bands are observed in each C=O stretch range, despite three (amide or ester) C=O bonds present in Bv, Bv is likely to take a symmetric conformation. Interestingly, the Na^+Bv solely shows a red-shifted band of ester C=O stretches by 30 cm^{-1}, suggesting a direct bonding between ester C=O and Na^+. The calculated IR spectra of the lowest-energy conformers are shown in Fig. 12a besides each experimental spectrum. The vibrational frequencies, splitting, and relative intensities of the bands observed are well reproduced by the calculated IR spectra of the minimum-energy structures. In the calculated structures, the ions except for Na^+ sit above the cavity of Bv and it is only bonded

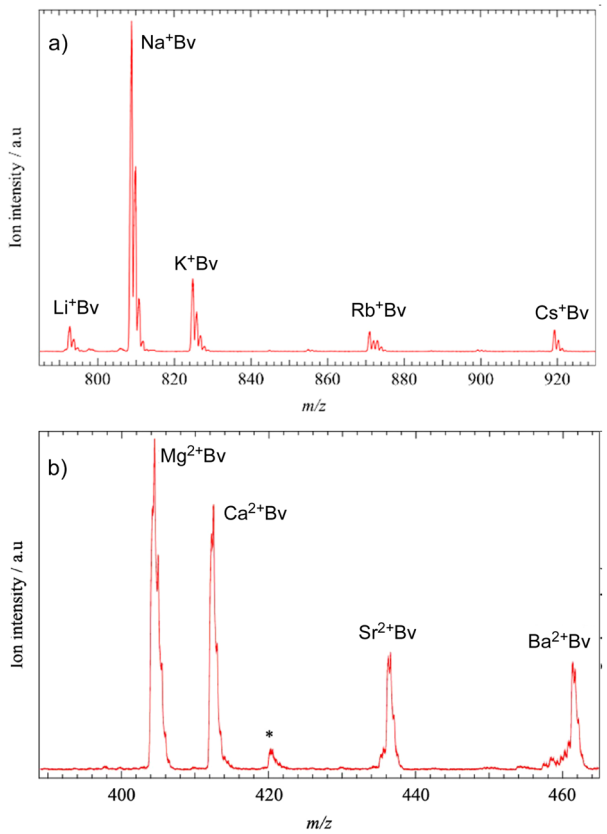

Fig. 11 ESI mass spectrum of the mixture containing Bv and (a) the five alkali metal ions and (b) the four alkaline earth metal ions with an equivalent concentration of Bv and each metal ion (1.0×10^{-5} M). Adapted with permission from refs. 69 and 70. Copyright 2022 and 2023 American Chemical Society.

by the three amide C═Os. In contrast, Na^+ is hexacoordinated by the three amide and ester C═Os, in which Na^+ is drawn inside the cavity. This tight binding by six C═O bonds can rationalize the preference of Bv to Na^+.

Another interesting point is that Bv favors amide coordination, whereas VM adopts the ester-bound bracelet structures. The optimized conformer in which an ion is coordinated by the three ester C═Os does not well reproduce the experimental IRPD spectra and is less stable by 50–60 kJ mol^{-1} than the most stable amide-bound conformer.[69] Because the conformational destabilization with the ester coordination is relatively small (<10 kJ mol^{-1}), the preference to amide C═Os can be primarily ascribed to the stronger binding energy between a metal ion and amide C═Os. This is in line with the fact that gas-phase binding energies of metal-amide (*e.g.* 202 kJ mol^{-1} for Li^+–*N*-methylacetamide) are higher than those of metal-ester (*e.g.* 180 kJ mol^{-1} for Li^+–methylacetate), as revealed by collision-induced dissociation mass spectrometry.[70] In contrast, VM favors the ester-bound bracelet structure, which is likely due to stabilization by the multiple intramolecular H-bonds.

We have measured the ESI mass spectrum of the 1 : 1 complexes of the Bv-alkaline earth metal ions as well (Fig. 11b).[71] The ESI spectrum shows a preference to physiologically abundant Mg^{2+} and Ca^{2+} over Sr^{2+} and Ba^{2+}. The IRPD spectra (Fig. 12b) exhibit amide and ester C═O stretches at 1600–1660 cm^{-1} and 1680–1770 cm^{-1}, respectively. The vibrational frequencies are in principle red-shifted compared with those of Bv-alkali metal complexes, probably due to the stronger vibrational Stark effects by divalent alkaline earth metals. These spectra also show the reduced number of C═O bands (except for Ba^{2+}), suggesting that the C_3-symmetric framework of Bv is retained as well for alkaline

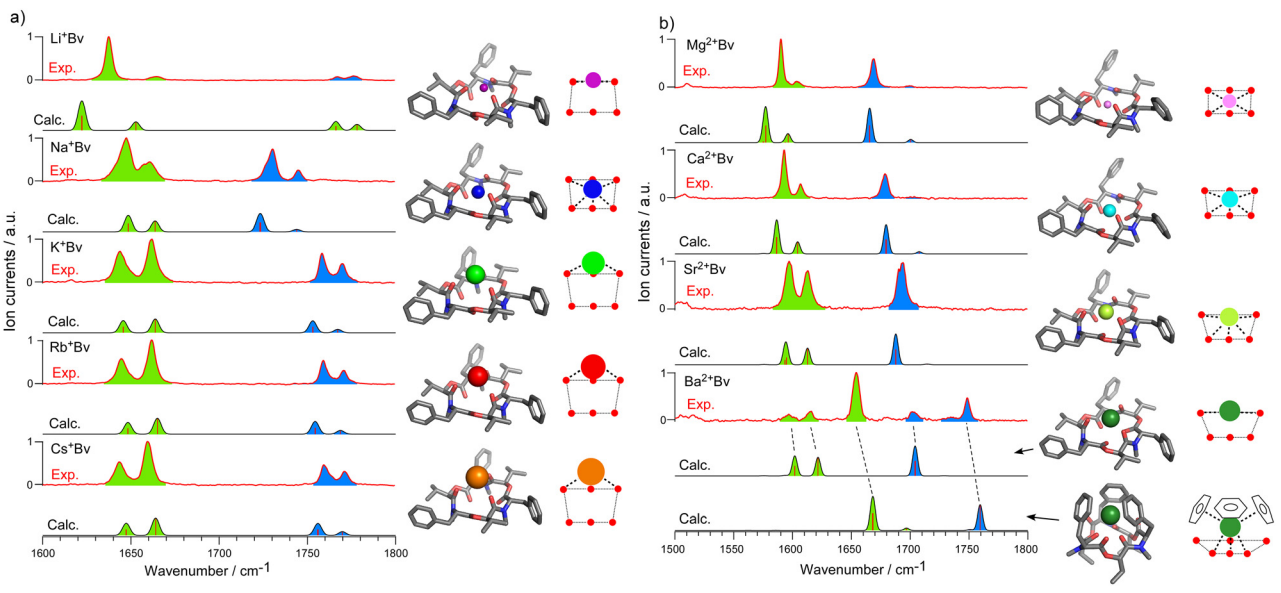

Fig. 12 IRPD (red) of (a) M^+Bv (M^+ = Li^+, Na^+, K^+, Rb^+, Cs^+) and (b) $M^{2+}Bv$ (M^{2+} = Mg^{2+}, Ca^{2+}, Sr^{2+}, Ba^{2+}) with calculated IR spectra of the lowest-energy conformers. The green and blue bands are assigned to amide and ester C═O stretches, respectively. The location of the ion relative to the six carbonyl oxygens (red circle) is also on the right side. The structural re-assignment of $Ba^{2+}Bv$ is based on ref. 71. Adapted with permission from ref. 69 and 70. Copyright 2022 and 2023 American Chemical Society.

earth metals. The vibrational signatures are well reproduced by the calculated IR spectra of the lowest-energy conformers other than Ba^{2+}. The assigned structures of Mg^{2+}Bv and Ca^{2+}Bv exhibit a hexacoordinated configuration, accommodating ions with a conformational motif similar to that of alkali metals. Sr^{2+}Bv shows a similar framework of Bv with an upshift in the position of the metal ion. For the Ba^{2+}Bv complex, the bands at 1595 cm^{-1}, 1615 cm^{-1}, and 1702 cm^{-1} are close to those observed in the other alkaline earth metal ions. These bands are assigned to the C_3-symmetric amide-bound structures with the identical binding motif as the other alkaline earth metals. The major bands at 1650 cm^{-1} and 1750 cm^{-1} were initially assigned[71] to metastable conformers in which an additional benzene ring participates in the coordination to Ba^{2+}. This has now been re-assigned to a stable C_3-symmetric conformer in which the metal is coordinated by three ester C═Os and stabilized by additional three cation-π interactions with benzene rings (Fig. 12b) with the help of ion mobility measurements.[72]

Fig. 13a summarizes the signed distances of the ions from the mean plane of the amide C═Os for each assigned structure as a function of ionic radius. Negative values indicate that a metal ion is located inside the cavity. Ions are pulled into the cavity as the ionic radius decreases. Li^+ appears to be an exception possibly due to its extremely small size and its ability to distort the Bv amide carbonyl ring. This trend is in line with the typical expected trend for the size-matching model, in which ionophores accommodate high-affinity ions inside the cavity when they show optimal fit with their ion sizes. In this sense, the ion selectivity of Bv for 1 : 1 complexes is adequately accounted for by the size-matching model apart from hydration, in sharp contrast to the case of VM composed of alternate amide/ester COs. The difference would be ascribed to the rigidity of the cavity, in which Bv shows the minimal expansion of cavity size, whereas VM expands its cavity volume almost twice when it binds to the largest Cs^+ (Fig. 14) due to the flexible backbone wireframe.

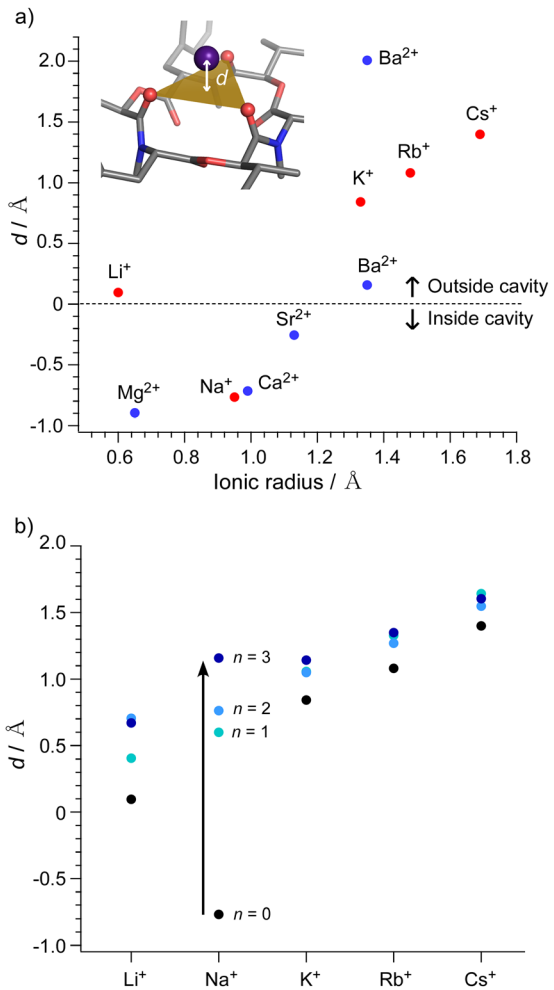

Fig. 13 Signed distances (d) between a metal ion and an amide plane of three amide oxygens for (a) $M^+Bv/M^{2+}Bv$ and (b) $M^+Bv(H_2O)_n$. Positive and negative values indicate that the ion is located outside and inside the cavity, respectively. The amide plane is defined as the plane containing the three amide oxygens. All the structures are optimized at the M06-2X/6-311++G(d,p) level.

3.2. Kinetic effects

As described in the Introduction, hydration affects not only the thermodynamic preference but also the kinetic transport rates in the catch, transport, and release processes (Fig. 3). Stepwise hydration of ionophore-ion complexes enabled by double ion trap spectroscopy provides a realistic mimic of such processes at the water–membrane interface. To this end, IRPD spectra of mono-hydrated Na^+Bv were measured (Fig. 15 and Fig. 16a).[73] Notably, the ester C═Os are blue-shifted by 30 cm^{-1} upon single water addition. This strongly suggests that Na^+ is no longer bonded by the ester C═Os. The vibrational bands at 1400–1800 cm^{-1} and 3400–3800 cm^{-1} are well reproduced by the calculations of minimum-energy conformers (Fig. 16a), which supports the hypothesis that the $Na^+Bv(H_2O)_1$ complex undergoes an upward

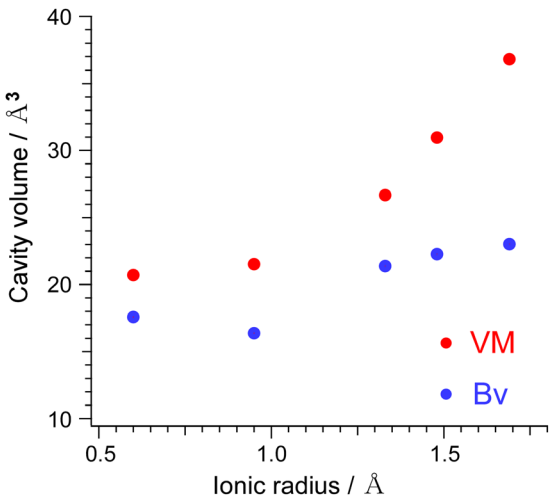

Fig. 14 Cavity volumes for M^+Bv and M^+VM (M = alkali metal). The cavity volume is defined as the convex hull of the six carbonyl oxygens forming the cavity.

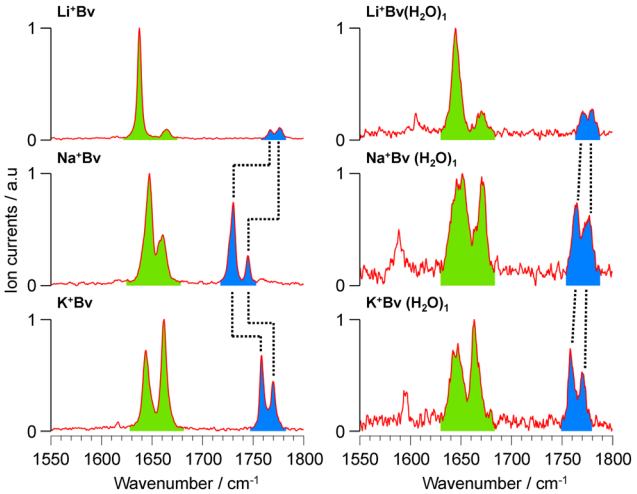

Fig. 15 IRPD spectra of M^+Bv and $M^+Bv(H_2O)_1$ (M^+ = Li^+, Na^+, K^+) in the 6 μm range. Reprinted with permission from ref. 72. Copyright 2024 American Chemical Society.

displacement of Na^+ accompanied by a reduction in coordination number (Fig. 16b). These results suggest that even a single water molecule is sufficient to initiate the ion release by pulling Na^+ out of the cavity and onto the amide C═O plane. In contrast, the IRPD spectra of the other mono-hydrated M^+Bv show little frequency shift in the ester C═O stretches, showing that Na^+ is susceptible to the hydration-induced structural change (Fig. 15). We have determined the conformations of higher hydrated $M^+Bv(H_2O)_n$ (n = 1–3) by comparing the experimental IRPD spectra with the calculated IR spectra.[74] Fig. 13b plots the distance from the mean amide C═O to a metal ion for hydrated clusters. This clearly shows that the position of Na^+ is most significantly shifted toward the upper rim and onto the amide plane upon micro-hydration. This can be attributed to the strong interaction of Na^+ with water, as discussed for VM. Unlike the case of VM, water is not inserted into the cavity but pulls Na^+ out of the cavity due to the smaller cavity size of Bv (Fig. 14). It should be noted that the hydration-induced structural change would impede the thermodynamically stabilities of Na^+Bv, apparently contradicting the high selectivity of Na^+ in methanol. Measurements of methanol-solvated Na^+Bv complexes would therefore be needed for further understanding.

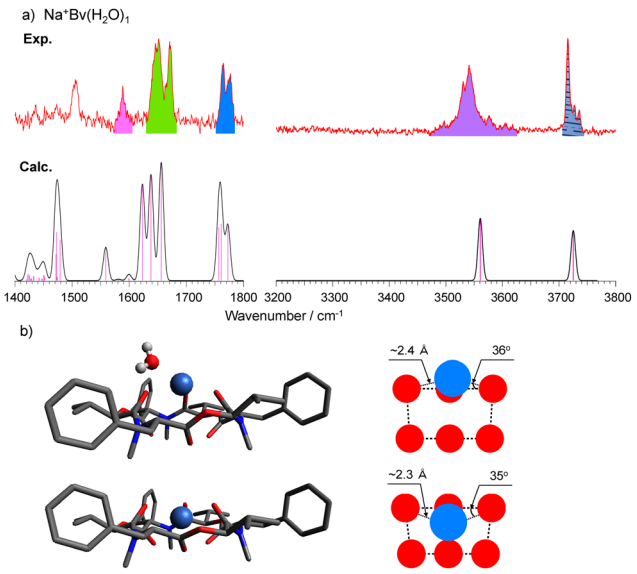

Fig. 16 (a) IRPD (red) of $Na^+Bv(H_2O)_1$ with calculated IR spectra (black) of the lowest-energy conformers. (b) The structural information on Na^+Bv and $Na^+Bv(H_2O)_1$. The green and blue bands are assigned to amide and ester C═O stretches, respectively. Reprinted with permission from ref. 72. Copyright 2024 American Chemical Society.

Another important aspect is that the transport rate inside the cell membrane would also be affected by water attachment, as proposed in our studies on VM. We evaluated the shape and size of the hydrated clusters using two geometric metrics: asphericity order parameter (A_3) and mean-squared radius of gyration (S^2).[30] Surprisingly, the dominant conformation of $K^+VM(H_2O)_1$ takes a more spherical and compact structure than the bare K^+VM complex, potentially enhancing the diffusion rate through the cell membrane. This suggests that complete dehydration is not required for ion transport. Instead, water can play an active role in the ion transport.

4. Conclusion

In this perspective, we review the micro-hydration effect on ion recognition revealed by cryogenic ion trap infrared spectroscopy. It was revealed that VM can capture different-sized metal ions by expanding its cavity volume in the absence of water. Single-water hydration drastically changed the molecular conformations of VM-metal complexes, leading to the emergence of the ion selectivity of VM. Hydration also alters the molecular conformations of 18C6 to realize size-fit type ion recognition by solidifying the framework of the crown ether. These hydration-induced structural changes arise from the intricate interactions among water molecules, an ion and an ionophore. Ionophores are subject to a certain constraint on their structural flexibility to maximize these interactions, confining a specific-sized ion. This finding reveals a new model for ion recognition in flexible ionophores such as VM and 18C6, deviating from the conventional size-matching model and suggesting a novel design principle for flexible ionophores. An advantage of these ionophores is that the ion selectivity can be tuned by the nature of the solvents. For example, 15-crown-5 ether exhibits a prominent solvent dependence on binding preference to alkali metal ions: it shows high affinity to Na^+ in acetonitrile, but to K^+ in methanol.[4] Such solvent dependence could be the next target of investigation.

Kinetic hydration effects are also proposed with the aid of ESI double ion trap IR spectroscopy. It has been revealed that Na^+ is pulled out of the cavity of Bv by the addition of a few water molecules, which suggests the acceleration of ion release by hydration at the water–membrane interface. Water may accelerate the transport rate as well by contracting the overall size of the ion-ionophore complexes. On the other hand, the kinetic rates for the individual catch, transport, and release steps remain scarce because conventional transport experiments only

monitor the overall flux of ions through a lipid membrane (or an organic layer), reflecting the outcomes of the three processes.[75] Advanced experimental approaches to directly probe these elementary processes help to bridge the gap between the macroscopic kinetics and microscopic hydration effects.

It should be emphasized that ion transport rates (or kinetic ion selectivity) do not necessarily match the thermodynamic preference. A high binding affinity for a certain ion may facilitate the capture process, but it can retard the ion release. In this sense, extraordinarily high thermodynamic stability may impede kinetic selectivity. A typical example is provided by K^+ channels, which selectively transport K^+ over smaller Na^+ and Li^+ across the cell membrane. The K^+ selectivity is achieved by a passageway formed by four identical subunits, known as the selectivity filter (SF).[76,77] Interestingly, MD simulations suggest that the impermeable Na^+ and Li^+ interact with the selectivity filter more strongly than K^+ due to their stronger charge densities,[78] which exemplifies a trade-off between thermodynamic stability and kinetic efficiency in ion transport. Furthermore, the role of water is a long-standing debate[79] in the ion transport of K^+ channels: hard knock-on and soft knock-on mechanisms. In the hard knock-on model, K^+ translocates through SF driven by Coulomb repulsion from the neighboring K^+.[80,81] In contrast, the soft knock-on mechanism proposes that K^+ and H_2O are alternatively located in SF to reduce the electrostatic repulsions.[77,82] Future research will be directed to how water modulates the thermodynamics and kinetics and its trade-off relations, including the more complex molecular systems such as K^+ channels.

Conflicts of interest

There are no conflicts to declare.

Data availability

Data sharing does not apply as no new data were measured in this perspective.

Acknowledgements

This work is supported in part by KAKENHI (JP25K01726) and the Core-to-core program of JSPS (JPJSCCA2024002), World Research Hub Initiative in the Institute of Science, Tokyo, Kurita Water and Environmental Foundation, and the Precise Measurement Technology Promotion Foundation (PMTP-F). The computations are performed at the Research Center for Computational Science, Okazaki, Japan (25-IMS-C095).

References

1 X. Yang, Q. Zhang, Y. Liu, M. Nian, M. Xie, S. Xie, Q. Yang, S. Wang, H. Wei and J. Duan, *et al.*, *Angew. Chem., Int. Ed.*, 2023, **62**, e202303280.
2 C. J. Pedersen, *Angew. Chem., Int. Ed. Engl.*, 1988, **27**, 1021–1027.
3 R. M. Izatt, R. E. Terry, D. P. Nelson, Y. Chan, D. J. Eatough, J. S. Bradshaw, L. D. Hansen and J. J. Christensen, *J. Am. Chem. Soc.*, 1976, **98**, 7626–7630.
4 R. M. Izatt, J. S. Bradshaw, S. A. Nielsen, J. D. Lamb, J. J. Christensen and D. Sen, *Chem. Rev.*, 1985, **85**, 271–339.
5 M. B. More, D. Ray and P. B. Armentrout, *J. Am. Chem. Soc.*, 1999, **121**, 417–423.
6 Y. Marcus, *J. Chem. Soc., Faraday Trans.*, 1991, **87**, 2995–2999.
7 N. Kikkawa, L. Wang and A. Morita, *J. Chem. Phys.*, 2016, **145**, 014702.
8 R. E. Smalley, L. Wharton and D. H. Levy, *J. Chem. Phys.*, 1975, **63**, 4977–4989.
9 N. Mikami, A. Hiraya, I. Fujiwara and M. Ito, *Chem. Phys. Lett.*, 1980, **74**, 531–535.
10 D. J. Miller and J. M. Lisy, *J. Am. Chem. Soc.*, 2008, **130**, 15381–15392.
11 T. G. Dietz, M. A. Duncan, D. E. Powers and R. E. Smalley, *J. Chem. Phys.*, 1981, **74**, 6511–6512.
12 G. Meijer, M. S. de Vries, H. E. Hunziker and H. R. Wendt, *Appl. Phys. B*, 1990, **51**, 395–403.
13 Y. Inokuchi, Y. Kobayashi, T. Ito and T. Ebata, *J. Phys. Chem. A*, 2007, **111**, 3209–3215.
14 H. Mitsuda, M. Miyazaki, I. B. Nielsen, P. Çarçabal, C. Dedonder, C. Jouvet, S. Ishiuchi and M. Fujii, *J. Phys. Chem. Lett.*, 2010, **1**, 1130–1133.
15 E. J. Cocinero, P. Carcabal, T. D. Vaden, J. P. Simons and B. G. Davis, *Nature*, 2011, **469**, 76–79.
16 O. V. Boyarkin, S. R. Mercier, A. Kamariotis and T. R. Rizzo, *J. Am. Chem. Soc.*, 2006, **128**, 2816–2817.
17 J. B. Fenn, M. Mann, C. K. Meng, S. F. Wong and C. M. Whitehouse, *Science*, 1989, **246**, 64–71.
18 X.-B. Wang and L.-S. Wang, *Rev. Sci. Instrum.*, 2008, **79**, 073108.
19 M. Z. Kamrath, E. Garand, P. A. Jordan, C. M. Leavitt, A. B. Wolk, M. J. Van Stipdonk, S. J. Miller and M. A. Johnson, *J. Am. Chem. Soc.*, 2011, **133**, 6440–6448.
20 Y. Inokuchi, O. V. Boyarkin, R. Kusaka, T. Haino, T. Ebata and T. R. Rizzo, *J. Am. Chem. Soc.*, 2011, **133**, 12256–12263.
21 N. S. Nagornova, T. R. Rizzo and O. V. Boyarkin, *Science*, 2012, **336**, 320–323.
22 J. G. Redwine, Z. A. Davis, N. L. Burke, R. A. Oglesbee, S. A. McLuckey and T. S. Zwier, *Int. J. Mass Spectrom.*, 2013, **348**, 9–14.
23 J. Jašík, J. Žabka, J. Roithová and D. Gerlich, *Int. J. Mass Spectrom.*, 2013, **354–355**, 204–210.
24 M. Broquier, S. Soorkia and G. Grégoire, *Phys. Chem. Chem. Phys.*, 2015, **17**, 25854–25862.
25 A. Günther, P. Nieto, D. Müller, A. Sheldrick, D. Gerlich and O. Dopfer, *J. Mol. Spectrosc.*, 2017, **332**, 8–15.
26 H. J. Eun, A. Min, C. W. Jeon, I. T. Yoo, J. Heo and N. J. Kim, *J. Phys. Chem. Lett.*, 2020, **11**, 4367–4371.
27 Z. Ma, L. Chen, C. Xu and J. A. Fournier, *J. Phys. Chem. Lett.*, 2023, **14**, 9683–9689.

28 S. Muramatsu, M. Koyama and Y. Inokuchi, *Chem. – Asian J.*, 2026, **21**, e70633.
29 B. M. Marsh, J. M. Voss and E. Garand, *J. Chem. Phys.*, 2015, **143**, 204201.
30 E. Sato, K. Hirata, J. M. Lisy, S. Ishiuchi and M. Fujii, *J. Phys. Chem. Lett.*, 2021, **12**, 1754–1758.
31 D. Nolting, C. Marian and R. Weinkauf, *Phys. Chem. Chem. Phys.*, 2004, **6**, 2633–2640.
32 G. Grégoire, C. Jouvet, C. Dedonder and A. L. Sobolewski, *J. Am. Chem. Soc.*, 2007, **129**, 6223–6231.
33 C. M. Choi, D. H. Choi, N. J. Kim and J. Heo, *Int. J. Mass Spectrom.*, 2012, **314**, 18–21.
34 S. Ishiuchi, H. Wako, D. Kato and M. Fujii, *J. Mol. Spectrosc.*, 2017, **332**, 45–51.
35 T. M. Chang, J. S. Prell, E. R. Warrick and E. R. Williams, *J. Am. Chem. Soc.*, 2012, **134**, 15805–15813.
36 J. W. DePalma, P. J. Kelleher, L. C. Tavares and M. A. Johnson, *J. Phys. Chem. Lett.*, 2017, **8**, 484–488.
37 H. Brockmann and G. Schmidt-Kastner, *Chem. Ber.*, 1955, **88**, 57–61.
38 D. Zhang, Z. Ma, H. Chen, Y. Lu and X. Chen, *Biomed. J.*, 2020, **43**, 414–423.
39 M. S. Frant and J. W. Ross, *Science*, 1970, **167**, 987–988.
40 K. Neupert-Laves and M. Dobler, *Helv. Chim. Acta*, 1975, **58**, 432–442.
41 S. Varma, D. Sabo and S. B. Rempe, *J. Mol. Biol.*, 2008, **376**, 13–22.
42 E. Grell, T. Funck and H. Sautee, *Eur. J. Biochem.*, 1973, **34**, 415–424.
43 F. Wang, C. Zhao and P. L. Polavarapu, *Biopolymers*, 2004, **75**, 85–93.
44 T. Dudev, D. Cheshmedzhieva, R. Dimitrova, P. Dorkov and I. Pantcheva, *RSC Adv.*, 2020, **10**, 5734–5741.
45 T. Dudev, D. Cheshmedzhieva, P. Dorkov and I. Pantcheva, *Molecules*, 2022, **27**, 532.
46 K. Hirata, E. Sato, J. M. Lisy, S. Ishiuchi and M. Fujii, *Phys. Chem. Chem. Phys.*, 2023, **25**, 1075–1080.
47 K. Hirata, E. Sato, J. M. Lisy, S. Ishiuchi and M. Fujii, *J. Phys. Chem. Lett.*, 2023, **14**, 5567–5572.
48 J. M. Lisy, *Int. Rev. Phys. Chem.*, 1997, **16**, 267–289.
49 R. Sakuma, K. Hirata, J. M. Lisy, M. Fujii and S. Ishiuchi, *J. Am. Chem. Soc.*, 2025, **147**, 45–50.
50 J. D. Rodriguez, T. D. Vaden and J. M. Lisy, *J. Am. Chem. Soc.*, 2009, **131**, 17277–17285.
51 J. D. Rodriguez and J. M. Lisy, *J. Am. Chem. Soc.*, 2011, **133**, 11136–11146.
52 J. D. Rodriguez, D. Kim, P. Tarakeshwar and J. M. Lisy, *J. Phys. Chem. A*, 2010, **114**, 1514–1520.
53 E. G. Buchanan, J. C. Dean, T. S. Zwier and E. L. Sibert, III, *J. Chem. Phys.*, 2013, **138**, 064308.
54 E. G. Buchanan, E. L. Sibert, III and T. S. Zwier, *J. Phys. Chem. A*, 2013, **117**, 2800–2811.
55 S. Lee, T. Wyttenbach, G. von Helden and M. T. Bowers, *J. Am. Chem. Soc.*, 1995, **117**, 10159–10160.
56 B. Martínez-Haya, P. Hurtado, A. R. Hortal, S. Hamad, J. D. Steill and J. Oomens, *J. Phys. Chem. A*, 2010, **114**, 7048–7054.
57 E. D. Glendening, D. Feller and M. A. Thompson, *J. Am. Chem. Soc.*, 1994, **116**, 10657–10669.
58 D. Feller, *J. Phys. Chem. A*, 1997, **101**, 2723–2731.
59 Z. Jing, G. Wang, Y. Zhou, D. Pang, F. Zhu and H. Liu, *J. Mol. Liq.*, 2020, **311**, 113305.
60 Z. Jing, Y. Zhou, T. Yamaguchi, K. Ohara, J. Pan, G. Wang, F. Zhu and H. Liu, *J. Phys. Chem. B*, 2023, **127**, 4858–4869.
61 R. L. Hamill, C. E. Higgens, H. E. Boaz and M. Gorman, *Tetrahedron Lett.*, 1969, **10**, 4255–4258.
62 Q. Wang and L. Xu, *Molecules*, 2012, **17**, 2367–2377.
63 Q. Wu, J. Patocka, E. Nepovimova and K. Kuca, *Front. Pharmacol.*, 2018, **9**, 1338.
64 F. Caloni, P. Fossati, A. Anadón and A. Bertero, *Environ. Toxicol. Pharmacol.*, 2020, **75**, 103349.
65 C. Al Khoury, N. Nemer and G. Nemer, *Sci. Rep.*, 2021, **11**, 10865.
66 R. W. Roeske, S. Isaac, T. E. King and L. K. Steinrauf, *Biochem. Biophys. Res. Commun.*, 1974, **57**, 554–561.
67 E. Makrlík, P. Selucký, P. Vaňura and P. Toman, *J. Inclusion Phenom. Macrocyclic Chem.*, 2012, **73**, 329–333.
68 Y. A. Ovchinnikov, V. T. Ivanov, A. V. Evstratov, I. I. Mikhaleva, V. F. Bystrov, S. L. Portnova, T. A. Balashova, E. N. Meshcheryakova and V. M. Tulchinsky, *Int. J. Pept. Protein Res.*, 1974, **6**, 465–498.
69 K. X. Vo, K. Hirata, J. M. Lisy, S. Ishiuchi and M. Fujii, *J. Phys. Chem. Lett.*, 2022, **13**, 11330–11334.
70 M. T. Rodgers and P. B. Armentrout, *Chem. Rev.*, 2016, **116**, 5642–5687.
71 K. X. Vo, K. Hirata, J. M. Lisy, S. Ishiuchi and M. Fujii, *J. Phys. Chem. A*, 2023, **127**, 7115–7120.
72 S. Kamioka, R. Ito, K. Ohshimo and F. Misaizu, *J. Phys. Chem. Lett.*, 2025, **16**, 7462–7469.
73 K. X. Vo, K. Hirata, J. M. Lisy, M. Fujii and S. Ishiuchi, *J. Phys. Chem. A*, 2024, **128**, 9159–9166.
74 K. X. Vo, K. Hirata, J. M. Lisy, M. Fujii and S. Ishiuchi, *J. Phys. Chem. A*, 2025, **129**, 8101–8109.
75 G. Stark, B. Ketterer, R. Benz and P. Läuger, *Biophys. J.*, 1971, **11**, 981–994.
76 D. A. Doyle, J. M. Cabral, R. A. Pfuetzner, A. Kuo, J. M. Gulbis, S. L. Cohen, B. T. Chait and R. MacKinnon, *Science*, 1998, **280**, 69–77.
77 Y. Zhou, J. H. Morais-Cabral, A. Kaufman and R. MacKinnon, *Nature*, 2001, **414**, 43–48.
78 K. Mita, T. Sumikama, M. Iwamoto, Y. Matsuki, K. Shigemi and S. Oiki, *Proc. Natl. Acad. Sci. U. S. A.*, 2021, **118**, e2017168118.
79 M. J. Ryan, L. Gao, F. I. Valiyaveetil, A. A. Kananenka and M. T. Zanni, *J. Am. Chem. Soc.*, 2024, **146**, 1543–1553.
80 W. Kopec, D. A. Köpfer, O. N. Vickery, A. S. Bondarenko, T. L. C. Jansen, B. L. de Groot and U. Zachariae, *Nat. Chem.*, 2018, **10**, 813–820.
81 P. S. Langan, V. G. Vandavasi, K. L. Weiss, P. V. Afonine, K. el Omari, R. Duman, A. Wagner and L. Coates, *Nat. Commun.*, 2018, **9**, 4540.
82 Y. Zhou and R. MacKinnon, *J. Mol. Biol.*, 2003, **333**, 965–975.